Colby College
Digital Commons @ Colby

Honors Theses | Student Research

2014

The Talbot Effect

Malia Kawamura
Colby College

Follow this and additional works at: https://digitalcommons.colby.edu/honorstheses

 Part of the Atomic, Molecular and Optical Physics Commons, Engineering Physics Commons, Optics Commons, and the Quantum Physics Commons

Colby College theses are protected by copyright. They may be viewed or downloaded from this site for the purposes of research and scholarship. Reproduction or distribution for commercial purposes is prohibited without written permission of the author.

Recommended Citation

Kawamura, Malia, "The Talbot Effect" (2014). *Honors Theses.* Paper 747.
https://digitalcommons.colby.edu/honorstheses/747

This Honors Thesis (Open Access) is brought to you for free and open access by the Student Research at Digital Commons @ Colby. It has been accepted for inclusion in Honors Theses by an authorized administrator of Digital Commons @ Colby.

Honors Thesis

The Talbot Effect

Author:

Malia Kawamura

Supervisor:

Professor Duncan A. Tate

Department of Physics and Astronomy

Colby College

May 15, 2014

Acknowledgments

Foremost, I want to sincerely thank Professor Duncan Tate of the Department of Physics and Astronomy at Colby College for all of his support and help. I really appreciate his willingness to advise my thesis on a subject that is outside of his normal research field because it was what I was most interested in researching. He did an excellent job balancing providing guidance and the opportunity to learn concepts on my own.

Second, I would like to thank Professor Ben McMorran of the Department of Physics at the University of Oregon. Ben welcomed me into his lab as a summer REU student and sparked my initial interest and understanding of the Talbot effect. All of the students in the McMorran lab were very helpful, but I would especially like to acknowledge Tyler Harvey for all his help fabricating gratings using e-beam lithography and Jordan Pierce for his assistance observing the Talbot effect in a TEM by volunteering the use of his own gratings. The work done on the electron Talbot effect at the University of Oregon was supported by the National Science Foundation under REU Grant No. CHE 1062512.

Finally, I am very grateful for the constant support of my family and friends. I could not have accomplished all of this work without them.

Abstract

The goal of this project is to experimentally investigate the optical Talbot effect and the electron Talbot effect. The Talbot effect is a near-field diffraction effect which occurs when plane waves are incident upon a grating. The Talbot effect creates full grating revivals at integral Talbot lengths and revivals with greater spatial periodicity at fractional Talbot lengths. We use a green helium neon laser and Ronchi rulings to take CCD camera images of the fractional Talbot revivals directly. Additionally, a photodiode records light intensity as a function of time as a second identical grating is moved to verify the presence of Talbot revivals. The camera and photodiode results are in good qualitative agreement with theory. We also obtain Talbot Lau revival images by using a sodium lamp as the incoherent light source.

To investigate the electron Talbot effect, we first fabricate 20 nm silicon nitride gratings using electron beam lithography. Then, in a transmission electron microscope (TEM) the Talbot effect is observed and quantified using a built-in TEM defocus function. TEM image analysis with Fiji confirms that fractional revivals appear as expected qualitatively. The TEM position readings of the Talbot revivals are not as theoretically expected, but this is likely due to uncertainty in the grating periodicity and the TEM defocus function. Further experiments could include fabricating smaller gratings using Talbot-assisted lithography and calibrating the TEM defocus function using the Talbot effect.

Contents

List of Figures

1 Introduction

1.1 Diffraction

Generally speaking, diffraction occurs when waves encounter an obstacle or aperture. The size scales between the wavelength of the wave and the obstacle or aperture must be comparable. Diffraction occurs in classical physics when waves bend around obstacles or when waves spread out from small openings. Diffraction also occurs in quantum physics with matter which has wavelike properties. An important historical example of diffraction is Thomas Young's double-slit experiment. In this experiment in the early 1800s, Young shone sunlight through two narrow slits as shown in Figure (1). The light diffracts through the first single slit and then as it diffracts through the double slit, the interaction of the waves is referred to as interference. The pattern on the screen of maxima and minima is a result of diffraction. This result was the first experimental evidence to disprove Newton's prevalent theory that light was made of particles. The maxima and minima pattern showed that instead light behaved as a wave. Later experiments in the 20th century showed that both matter and light can behave as waves with similar diffraction and interference experiments.

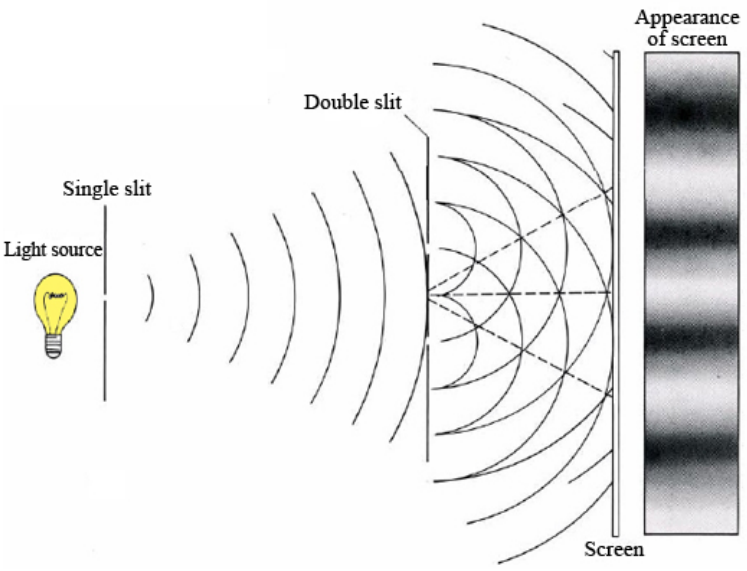

Figure 1: A schematic of Thomas Young's double slit experiment [1].

1.2 Near-Field Versus Far-Field Diffraction

In optics, diffraction behavior is classified by whether it is occurs in the near-field or the far-field. The near-field is close an aperture where the wavefront curvature is important. The far-field is farther away from an aperture where the wavefronts can be estimated as parallel. Diffraction that occurs in the far-field is called Fraunhofer diffraction and diffraction that occurs in the near-field is called Fresnel diffraction. Formally, Fraunhofer diffraction occurs when

$$\frac{a^2}{L\lambda} << 1 \tag{1.2.1}$$

and Fresnel diffraction occurs when

$$\frac{a^2}{L\lambda} >> 1 \tag{1.2.2}$$

where a is the aperture or slit size, L is the distance from aperture, and λ is the wavelength [2]. Young's double slit experiment is an example of far-field diffraction. Meanwhile, the Talbot effect occurs in the near-field. In the near-field, Fresnel approximations are made and the wavefront curvature cannot be ignored.

1.3 The Talbot Effect

The Talbot effect is a near-field diffraction effect in which incident plane waves on a periodic structure produce self-images or Talbot revivals. While inventing photography in 1836, Henry Fox Talbot discovered this effect which was later named after him [3]. In 1881, Lord Rayleigh explained the Talbot effect as a natural consequence of Fresnel diffraction [4]. The distance at which self-images of the periodic structure reappear due to constructive interference is called the Talbot length. Rayleigh showed that the Talbot length is a given by

$$L_T = \frac{d^2}{\lambda} \tag{1.3.1}$$

where d is the grating pitch and λ is the wavelength. Self-images of the grating appear shifted by half a period at every other Talbot length. At half Talbot lengths, there are twice as many Talbot revivals, showing a doubling of the grating pitch. At quarter Talbot lengths there are four times as many Talbot revivals and so on. Therefore, the interference pattern behind a grating is often referred to as a Talbot carpet as can be seen in Figure (2).

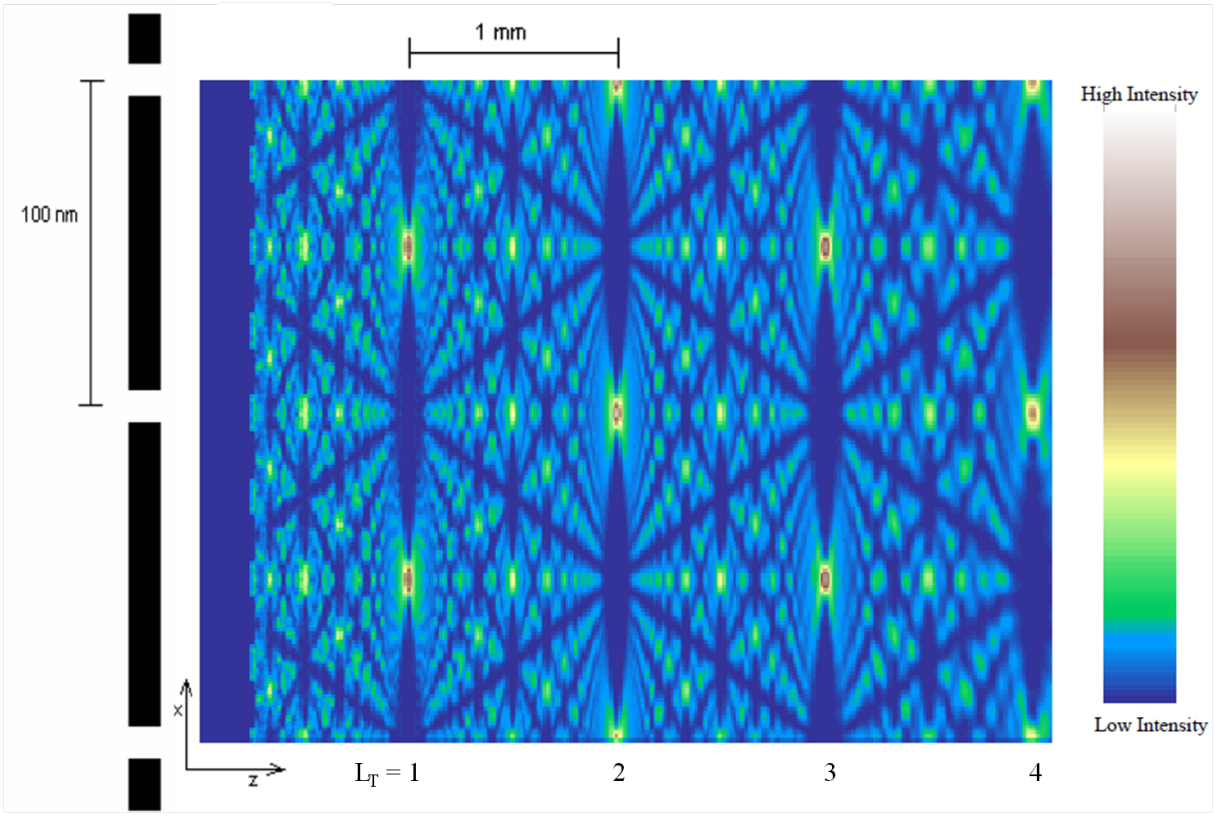

Figure 2: A theoretical Talbot carpet image generated with Igor Pro of a grating with a 100 nm pitch and 10 nm windows shown in black on the left. The atomic wavelength is 0.01 nm. The Talbot revivals can be seen at each Talbot length and the fractional revivals are visible as well. [4]

The Talbot effect can be observed with both light and atoms. To observe the optical Talbot effect a coherent light source, such as a laser, is required. Light is coherent if it is monochromatic (single wavelength) and in phase. This effect can also be observed with matter due to the wave nature of particles. For instance, the Talbot effect has been realized with both atoms [5] and electrons [6]. The Talbot effect has also been realized with surface plasmons by Mark Dennis of Bristol Theoretical Physics [7] and with surface plasmon polaritons by Alexei Maradudin at the University of California [8]. The diffraction effect is of interest because of its possible applications in atom lithography to create smaller structures at fractional Talbot lengths [5]. Additionally, phase imaging is of interest especially for medical applications [9, 10]. Atsushi Momose's group at the University of Tokyo, for example, focuses on X-ray Talbot interferometry to observe soft tissues and cartilage [9]. There are also applications of the Talbot effect in other fields beyond traditional optics such as acoustics, Bose-Einstein condensates, electron microscopy, x rays, nonlinear optics, and quantum optics [11].

1.4 This Thesis

This thesis includes research conducted at Colby College and at the University of Oregon. First, I will discuss work conducted at Colby College with Professor Duncan Tate studying the optical Talbot effect and the Talbot Lau effect. This research was done from the fall of 2013 through the spring of 2014. I will explain the three different optical apparatuses I built and the experimental results from each. Then, I will discuss work conducted at the University of Oregon with Professor Ben McMorran studying the electron Talbot effect. The research at the University of Oregon was completed as part of a physics REU program during the summer of 2013. I will give a detailed explanation of how to nanofabricate gratings using electron beam lithography, how I observed the electron Talbot effect in a transmission electron microscope, and how I analyzed the images using Fiji.

2 Optical Talbot Effect

The Talbot effect can be observed with both light and atoms. In this section, I will focus only on experiments with light. To observe the Talbot effect, coherent light must be used. A light source is coherent when the waves are in phase with each other across the emitted beam profile, like a laser. Meanwhile, incoherent light is required for the Talbot Lau effect. Incoherent light sources, like a standard light bulb, have light waves with no temporal or spatial correlation and can have different wavelengths. The Talbot effect and Talbot Lau effect are very similar. Both effects are due to near-field diffraction and result in self-image revivals. The main difference between the two effects is whether the light source is coherent or incoherent. To see both of these optical diffraction effects, amplitude gratings, gratings with complete open slits, are used. It is important to use amplitude gratings rather than phase gratings so that the phase of the light waves is not affected by the grating.

The goal of this section is use helium neon lasers as coherent light sources to directly and indirectly observe the optical Talbot effect. Fractional and complete Talbot revivals will be obtained directly using a camera. Then, a photodiode will indirectly confirm the presence of Talbot revivals by moving a second identical grating at one Talbot length behind the first grating. Next, a sodium lamp will be used as an incoherent light source to observe the Talbot Lau effect. Images of Talbot Lau revivals will also be captured with a camera.

2.1 Camera Apparatus and Results

To view the Talbot effect revivals directly, the laser and camera setup shown in Figure (3) is used. A green 543.5 nm helium neon (HeNe) laser is used with a beam expander. The polarized beam splitter (PBS) and neutral density (ND 20) filter are placed in the beam to reduce the number of photons that reach the camera to prevent it from damage. A 10 lines/mm grating (G) is placed on a hand operated translation stage to allow the distance (d) between the grating and the camera to be precisely adjusted. The grating is a Ronchi ruling with 10 lines/mm and 50% open fraction, which means that there is the same amount of open space as there is blocked space. The camera is a ThorLab's CMOS (complementary metal oxide semiconductor) color camera (DCC1645C) with a frame of view of 4.61 mm

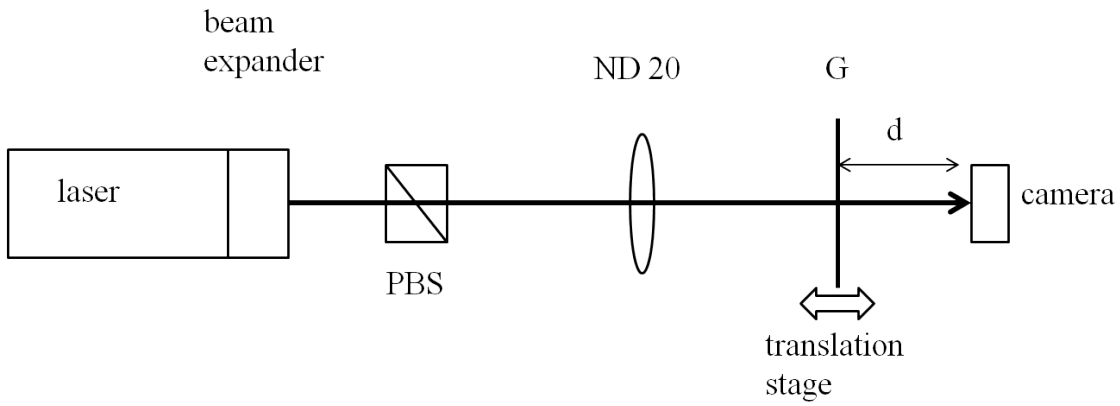

Figure 3: A schematic of the optical Talbot effect camera setup. A helium neon laser shines through a beam expander, polarized beam splitter (PBS), neutral density filter (ND 20), and grating (G) before reaching the camera.

by 3.64 mm. The camera is used without a lens so the revivals are imaged directly. To obtain images, the grating is moved slowly and many images are taken the with camera. Different numbers of lines are expected to appear due to the Talbot effect when the grating is placed at different distances (d). The expected Talbot length for the green HeNe laser and 10 lines/mm gratings is 1.84 cm. Therefore, separations of d range from 1.5 cm to 4.0 cm by increments of 0.1 cm to throughly image from one Talbot length to two Talbot lengths.

With the camera setup shown in Figure (3), camera images are captured at many fractional Talbot lengths. Figure (4) displays an exact grating replica at one Talbot length and as the distance increases additional Talbot revivals appear until at two Talbot lengths when the original grating revival returns. The double and triple times the number of revivals occur in approximately the expected locations. Yet, the quadruple Talbot revivals are expected to appear at about 1.25 L_T and 1.75 L_T. The reason for the location discrepancy is unknown. Nevertheless, the other revivals appear as expected.

To exemplify how the revival in Figure (4f) does have triple the periodicity of the revival at one Talbot length (Figure (4a)), a line profile plot is displayed in Figure (5). Fiji, an image processing program from ImageJ, is used to create the plot. First a line is drawn across the area of interest, which in this case is simply a line perpendicular to the visible

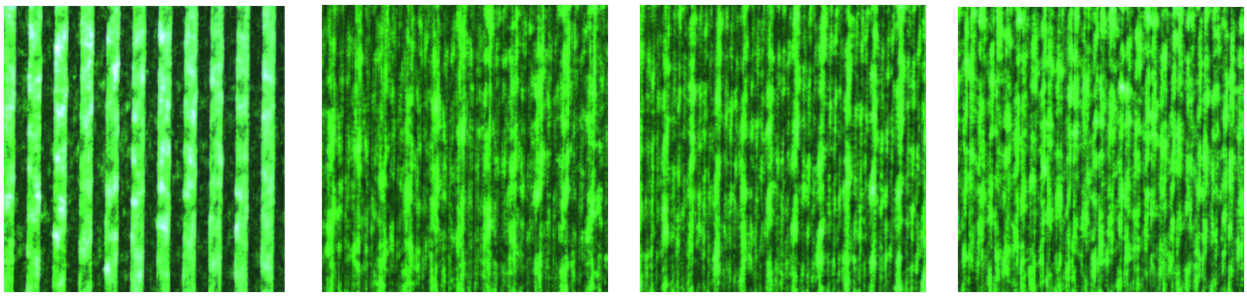

(a) 1x lines at 1 L_T (b) 3x lines at 1.31 L_T (c) 4x lines at 1.36 L_T (d) 2x lines at 1.5 L_T

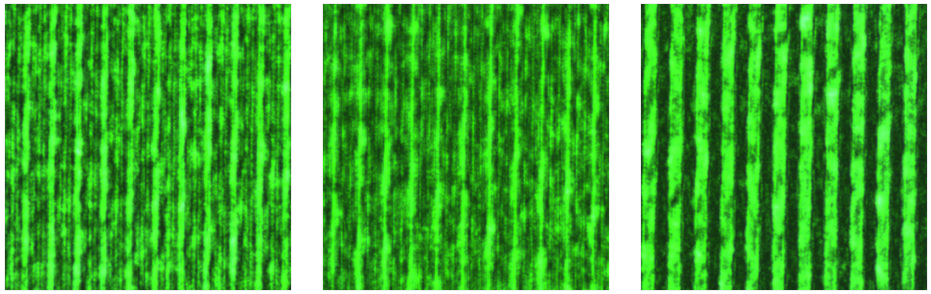

(e) 4x lines at 1.64 L_T (f) 3x lines at 1.70 L_T (g) 1x lines at 2 L_T

Figure 4: Camera images at different Talbot lengths showing double, triple, and quadruple Talbot revivals.

bright and dark lines. Then, a line profile is taken which calculates the pixel values at each location along the drawn line. Finally, these pixel values are plotted versus pixels to give Figure (5). From this line profile plot, the triple periodicity at 1.70 L_T compared to the periodicity one Talbot length is clear.

2.2 Photodiode Apparatus and Results

To detect Talbot revivals indirectly, a slightly different setup with a photodiode and oscilloscope is used. Figure (6) is a schematic of the photodiode apparatus. The goal of this setup is to obtain precise information about the spatial variation of interference fringes using two gratings. Green (543.5 nm) and red (632.8 nm) HeNe lasers are used with a beam expander. The two gratings (G1 and G2) are Ronchi rulings of either 10 lines/mm or 20 lines/mm. Some experiments are done with G1 and G2 both as 10 lines/mm gratings and other experiments are done with G1 as a 10 lines/mm grating and G2 as a 20 lines/mm grating. G1 is on a rotation mount so that it's lines can be aligned vertically precisely with

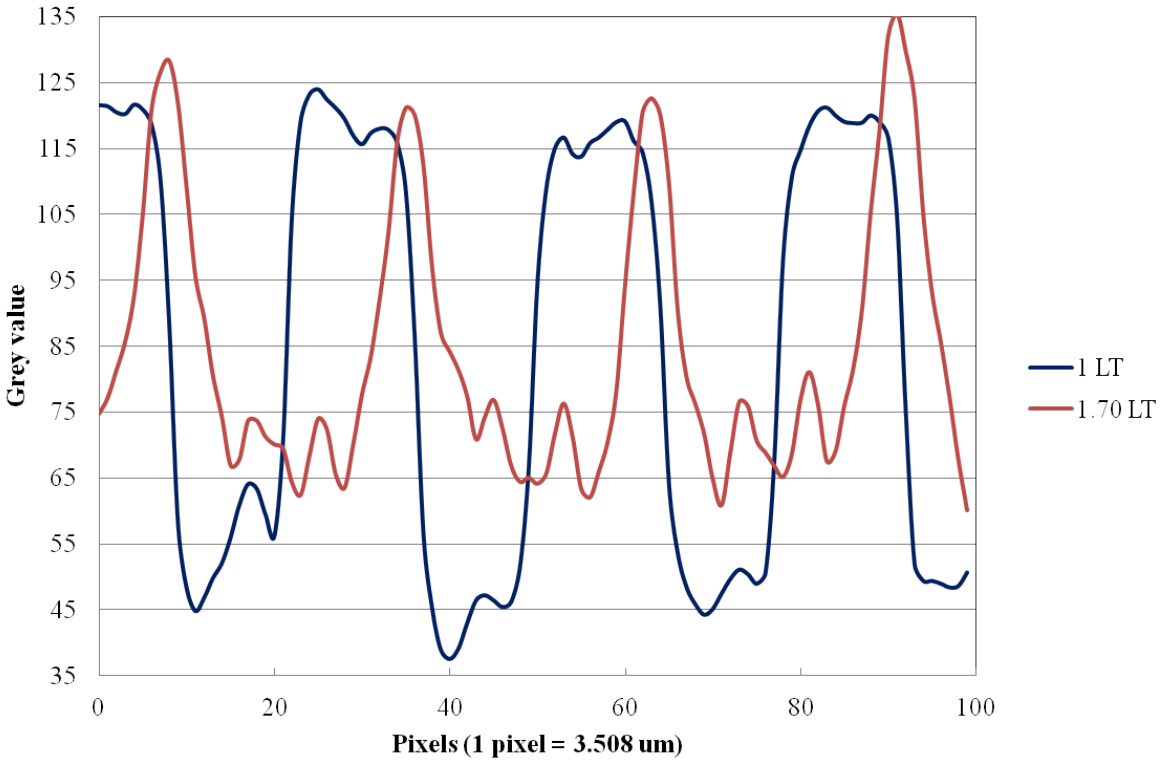

Figure 5: A line profile plot of 1 L_T and 1.70 L_T to clearly show the triple periodicity present at 1.70 L_T in Figure (4f). The relationship between pixel size and distance is estimated by the known periodicity of the revivals and the known grating pitch.

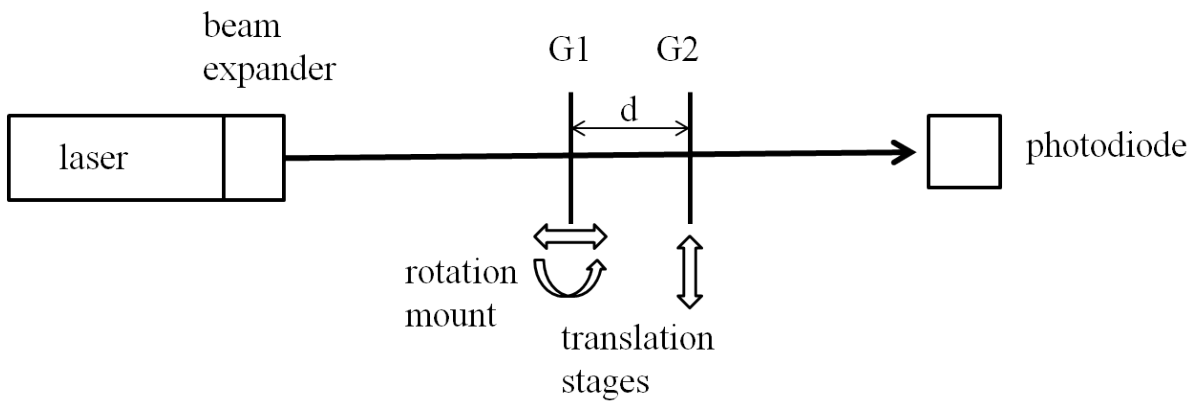

Figure 6: A schematic of the optical Talbot effect photodiode arrangement with two gratings (G1 and G2).

G2's lines which are perpendicular to the table. G1 is also on a hand operated translation stage so that the distance (d) between G1 and G2 can be adjusted. Then, G2 is on a motorized horizontal translation stage for which the translation velocity perpendicular to the laser beam can be precisely controlled. The motorized translation stage is a Newport Universal Motion Controller / Driver, Model ESP 300. Finally, there is a photodiode which transmits the incident photon information to an oscilloscope which provides the data as voltage values as a function of time.

The programmable jog velocity of the translation of G2 allowed for predictions of the frequency of peaks of the oscilloscope voltage based on how often the gratings would align. For example, with G1 and G2 both being 10 lines/mm exactly one Talbot length apart and the jog velocity of G2 set to move at 0.1 mm/s, the second grating moves by 1 line/s. Therefore, a minimum intensity is expected every 1 second. Due to an exact Talbot revival of the grating at one Talbot length, a second identical grating should be able to block almost all the light or let almost all the light through. Therefore, minima near zero volts are expected. Different distances (d) between gratings are explored as well.

For the setup in Figure (6) with a green (543.5 nm) HeNe laser and two 10 lines/mm gratings, the gratings are placed about 1.84 cm apart or one Talbot length apart. Then, while the photodiode is on and connected to an oscilloscope, the automated translation stage moves the second grating (G2) at 0.1 mm/s. For a jog velocity of 0.1 mm/s and a grating

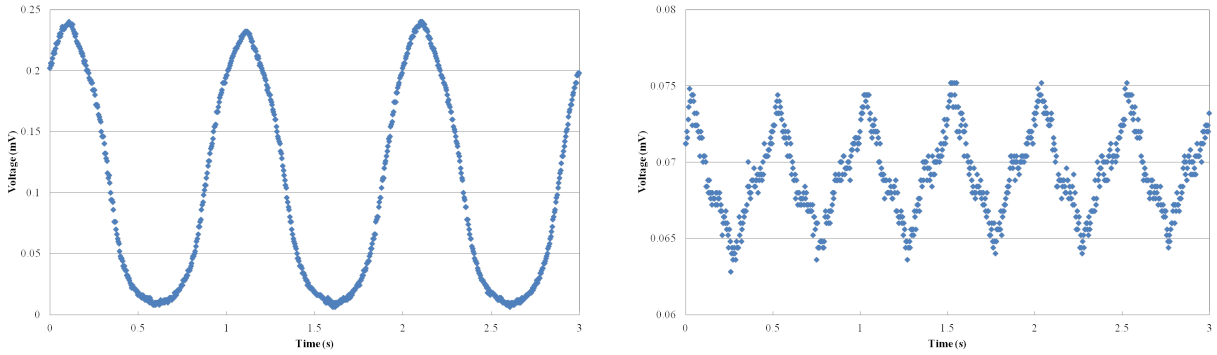

(a) $G1 = 10$ l/mm and $G2 = 10$ l/mm (b) $G1 = 10$ l/mm and $G2 = 20$ l/mm

Figure 7: Photodiode voltage versus time plots for G1 and G2 spaced at 1 L_T.

with line spacing of 10 lines/mm, it means that the grating should move by 1 line per second. In other words, G1 and G2 should align exactly every 1 second. In Figure (7a), voltage in mV from the oscilloscope is plotted versus time in seconds. Figure (7a) shows the alignment does occur exactly every second. The maxima occur when G1 and G2 are exactly aligned. There are maxima when the gratings are aligned because at one Talbot length behind the first grating (which is exactly where the second grating is), exact Talbot revivals are phase shifted by half a period as can be seen in Figure (2) so that most light is let through. Therefore, the minima in Figure (7a) occur when the gratings are exactly unaligned since then the second grating blocks the Talbot revivals nearly completely. This is an important result because it demonstrates indirectly how precisely refocused the light is behind the first grating that a second identical grating can block almost all of it. Another key result is that as the second grating is translated, the expected frequency of maxima and minima occur every one second as expected. Extremely similar results occur with a red (632.8 nm) HeNe laser in the same setup.

Next, still using the same photodiode setup in Figure (6), the second grating is changed to a 20 lines/mm grating. The gratings are still placed at one Talbot length apart ($d = 1.84$ cm) and the second grating is still translated at 0.1 mm/s. Yet, since the second grating has twice the pitch, it is expected that the maxima will occur twice as frequently (every 0.5 seconds). Figure (7b) shows that indeed with G2 as a 20 lines/mm grating, the maxima do occur every 0.5 seconds.

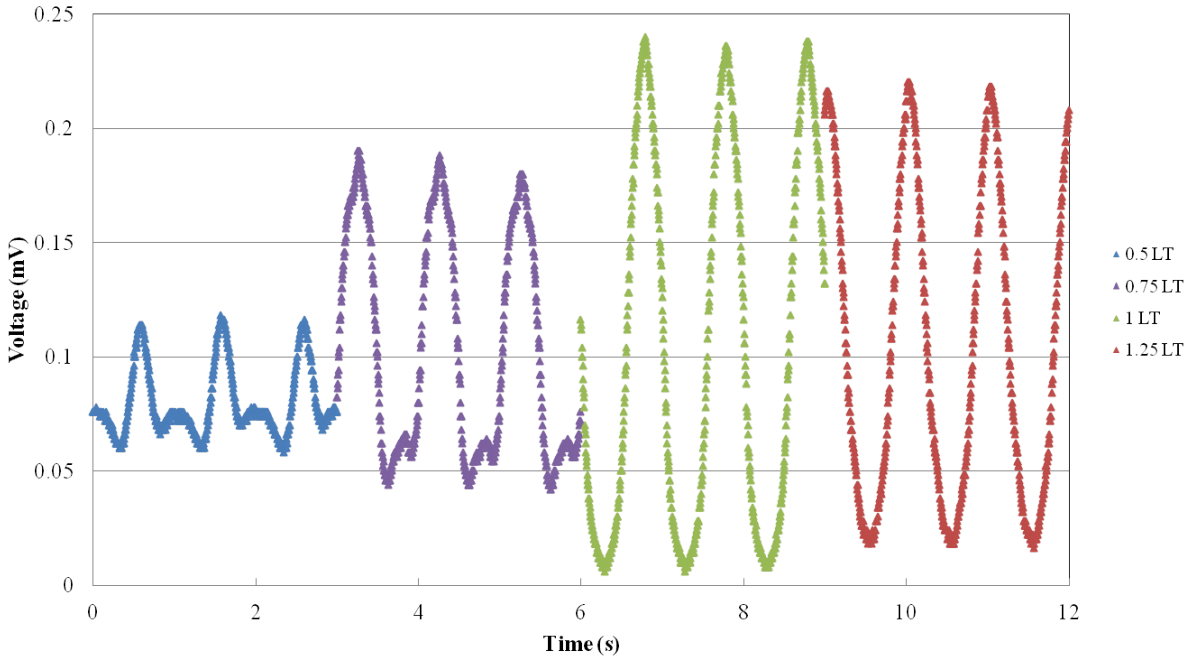

Figure 8: A graph comparing photodiode voltages with varying distances between the gratings of 0.5 L_T, 0.75 L_T, 1.0 L_T, and 1.25 L_T.

Next, with two 10 lines/mm gratings, the distance d between the gratings is varied. Figure (8) shows voltage versus time as the second grating is translated by 0.1 mm/s. The time scale on the y-axis is accurate in the sense that it represents seconds, but the data is not taken continuously as it appears. Instead, the distances are set at 0.5 L_T, 0.75 L_T, 1.0 L_T, and 1.25 L_T and time series data is taken with the second grating translating at 0.1 mm/s for each distance. Since the same translation speed and gratings are used, minima still occur every one second as expected regardless of the distance d. The different distances are combined in Figure (8) to display how the intensities change with grating spacing distance. At 1.0 L_T, the maxima and minima are most extreme as expected. Meanwhile, at other fractional Talbot distances, there is less extreme contrast as the second grating is translated because the second grating is not in a position where the light repeats with the same periodicity as the grating as it does at one Talbot length.

2.3 Talbot Lau Effect Apparatus and Results

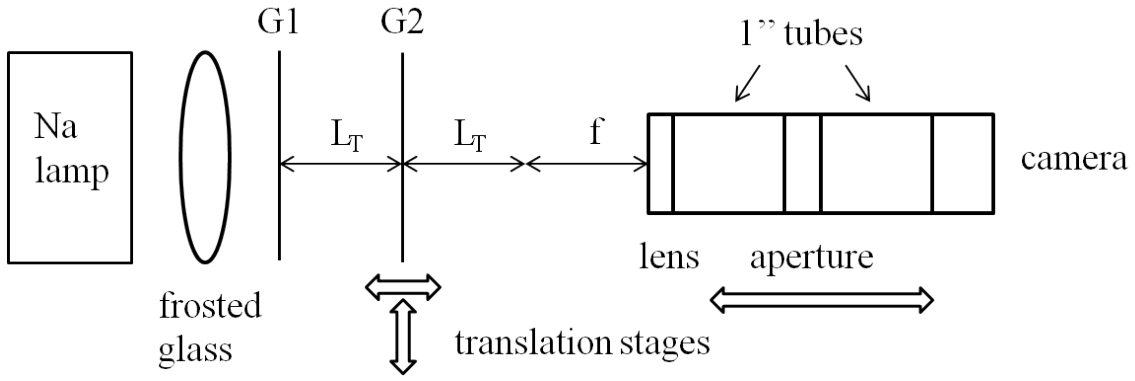

Figure 9: A schematic of the Talbot Lau setup with a sodium lamp where L_T is the Talbot length and f is the focal length.

The Talbot Lau effect is closely related to the Talbot effect as it is also a near-field self-imaging effect. The main difference between the Talbot Lau effect and Talbot effect is that the Talbot Lau effect occurs with incoherent light. Yet, in order to have self-imaging from incoherent light a second identical grating must be added behind the first grating. The second grating refocuses the waves to form a clear grating image which would not be visible with only a single grating [12]. We follow William Case's Talbot Lau work at the University of Vienna [12]. Like Case, we use a sodium lamp as our incoherent light source. The frosted glass transforms the sodium lamp light into a spatially incoherent beam. The gratings, G1 and G2, are 10 lines/mm Ronchi rulings. We use the same ThorLab's DCC1645C camera, but now additionally we use two 1" tubes, an aperture, and a lens. The tubes and lens are used to increase the magnification to approximately four times. The aperture remains nearly open and does not seem to have a large effect on the images. A lens with a 15 mm focal length is used.

To observe the Talbot Lau self-images, the camera focal length must be known precisely. Experiments with the camera, lens, tubes, and aperture are conducted to determine that the focal length is about 1.65 cm for the setup used in Figure (9). Then, the Talbot length for nearly monochromatic sodium light is about 1.70 cm using a wavelength of 589.3 nm and grating pitch of 0.1 mm. These distances need to be exact to observe the revivals and are

easily adjusted using two translation stages parallel to the beam to move both the camera and second grating. The second grating is also on a translation stage perpendicular to the beam so that the two gratings can be aligned.

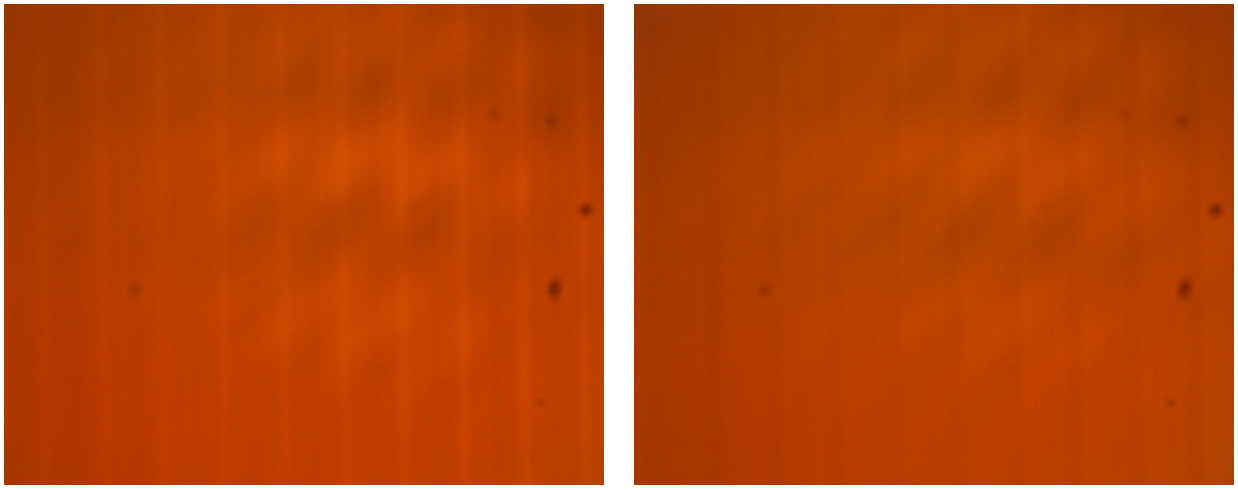

Figure 10: Talbot Lau fringes taken at approximately 1 L_T behind the second grating.

For the Talbot Lau effect, self-images of the gratings are harder to see than for the Talbot effect. Figure (10) shows revival images taken at one Talbot length behind the second grating. Theoretically, at one Talbot length an exact, to scale, grating revival should be visible as we showed for the Talbot effect in Figure (4a). Many minor modifications to the distances are conducted, but no better images were obtained. A main issue that makes the revivals difficult to see is the fact that the sodium lamp emits at two wavelengths so the Talbot length is not accurate for all the light. Nevertheless, the faint vertical visible lines are due to the Talbot Lau effect. In the future, period doubling should be visible using this setup by changing the two Talbot length distances (L_T) to 0.5 L_T.

3 Electron Talbot Effect

The work done to study that electron Talbot effect was conducted at the University of Oregon's Physics department in Ben McMorran's lab. The McMorran lab studies electron optics, matter wave optics, and electron microscopy. A main focus of the McMorran lab is electron vortices with quantized orbital angular momentum (OAM). The group manufactures very precise forked nanoscale diffraction holograms to make these electron vortices. The electron beams carrying OAM are of interest for improved imaging of magnetic and biological samples. For Ben's doctoral thesis at the University of Arizona he investigated the Talbot effect and built a Talbot interferometer in addition to many other experiments. With this background, Ben suggested that I study the electron Talbot effect in a transmission electron microscope (TEM) because that was something that he was interested in trying, but had never done and was an interesting demonstration of the wavelike nature of matter.

For this experiment, the electron Talbot effect is investigated using a TEM. Nanoscale gratings are used so that the periodicity of the grating is near the same order of magnitude as the wavelength of the accelerated electrons in the TEM. Grating pitch, d, is the center to center distance between grating slits. To determine the grating pitch needed, first the wavelength of the electrons in the TEM can be computed using the deBroglie wavelength equation

$$\lambda = \frac{h}{p} = \frac{h}{mv} \tag{3.0.1}$$

in which λ is the electron wavelength, h is Planck's constant, p is linear momentum, m is mass, and v is velocity. Then, the velocity of an electron is known by its kinetic energy such that

$$v = \sqrt{\frac{2E}{m}} \tag{3.0.2}$$

where E is the kinetic energy. Thus, equations 3.0.1 and 3.0.2 combine such that the wavelength of the electrons in the TEM is

$$\lambda = \frac{h}{\sqrt{2mE}} \frac{1}{\sqrt{1 + \frac{E}{2mc^2}}} \tag{3.0.3}$$

where c is the speed of light and the second term accounts for electrons traveling at relativistic speeds [13]. The Titan TEM accelerates electrons at 300 kV providing electrons with an

energy of 300 keV [14]. A TEM works the same way as a light microscope, it just uses electrons instead. The electrons have a shorter wavelength than light which allows for greater spatial resolution than optical microscopes. The 300 keV electrons have a wavelength of 1.97 pm given by equation 3.0.3 which is much shorter than visible wavelengths used in an optical microscope of about 500 nm. Since this experiment uses 200 μm thick silicon nitride samples, $L_T = 200$ μm and $\lambda = 1.97$ pm require that $d = 19.8$ nm.

3.1 Electron Grating Fabrication

The electron gratings are fabricated using electron-beam lithography in the Center for Advanced Materials Characterization in Oregon (CAMCOR) [15]. The gratings are silicon nitride because silicon nitride is structurally stable and chemically inert. Samples are obtained from a local Eugene company, Dune Sciences, which custom makes silicon samples with four 60 μm by 100 μm silicon nitride windows for the McMorran lab group. Electron-beam or e-beam lithography is the process of exposing an electron sensitive film with a scanning focused electron beam. Hafnium oxide sulfate (HafSOx) is a negative resist which means that anywhere the electron beam exposes the film or resist, the HafSOx polymerizes and adheres to the silicon nitride surface. After exposure, an etch of tetramethyl ammonium hydroxide (TMAH) develops the grating by removing the HafSOx layer anywhere it was not exposed to the electron beam. The fabrication process involves an optical microscope, sonicator, plasma cleaner, spin coater, scanning electron microscope (SEM), carbon coater, and atomic force microscope (AFM). Theoretically, this grating fabrication process will produce high quality gratings. Unfortunately, the gratings produced during my ten weeks at the University of Oregon did not produce high efficiency gratings. Nevertheless, the fabrication process is educational will be described since it should theoretically work with more practice and dose tests on scanning electron microscope (SEM).

3.1.1 Optical Microscope

To begin fabricating silicon nitride gratings, the 20 nm thick silicon nitride windows must be checked ensure that they are still intact using the Leica optical microscope. Broken windows

are sometimes easy to identify by their shattered, uneven, and black surfaces. Intact windows are also sometimes obvious with their light grey color and few specks of dust visible on the surface. At other times, whether a window is broken or intact is difficult to identify, but it is often helpful to examine the corners of the windows. Additionally, it is useful to compare known broken windows to unknown windows. A backlight on the microscope would be helpful as well.

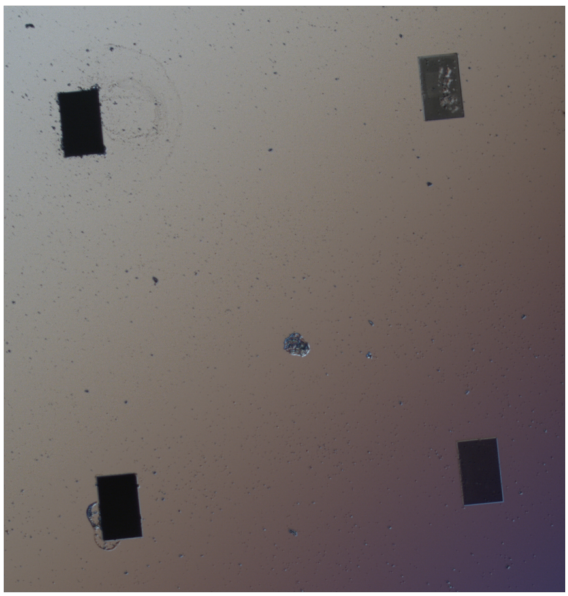

(a) Four 60 μm by 100 μm silicon nitride windows which are 20 nm thick.

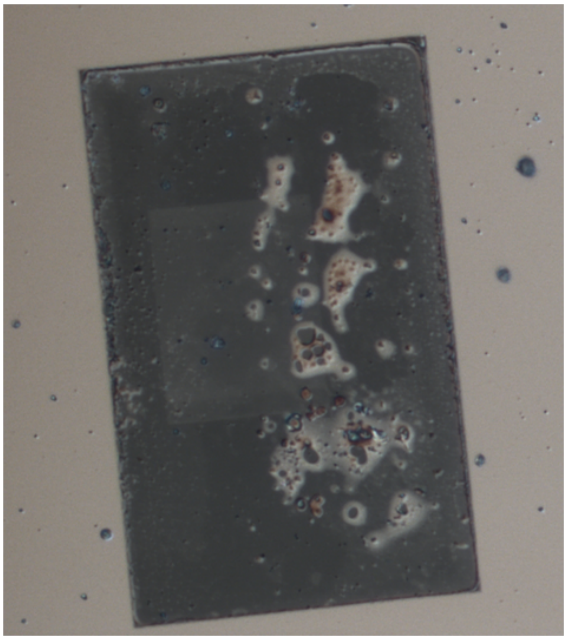

(b) Top right 60 μm by 100 μm window with 20 nm line pattern.

Figure 11: An optical microscope image of a set of four windows. The two windows on the left can be identified as broken by their dark black color and uneven corners. The two right windows are intact as can be seen by the light grey color and pattern visible on the top right window. The zoomed in image on the right shows a successfully patterned window. The window unfortunately shows residual contamination likely from the TMAH etch.

After a window is patterned, the optical microscope has sufficient resolution to easily view any patterns on the windows. Once again, the microscope can also identify broken windows. Figure (11) serves as an example of how broken, intact, and patterned windows look in the optical microscope.

3.1.2 Sonicator

The sonicator in the CAMCOR semiconductor room is the first step to clean the silicon nitride samples. A sample is placed in a small beaker with a sufficient amount of acetone to completely submerge the sample. Then, the beaker is held with a plastic scissor clamp and placed in the sonicator for approximately six minutes. Next, the sample is transferred to another small beaker with ispropyl alcohol (IPA). During the transfer, the sample must be sprayed with IPA continuously to prevent acetone from drying on the sample. Again, the sample is held in the sonicator with a plastic scissor clamp for about six minutes. After the IPA sonication, the sample is blow dried with nitrogen. The goal of sonication is to clean the surface of the sample. Yet, it was learned that sonication often causes the fragile 20 nm thick silicon nitride windows to shatter and so this cleaning step was removed.

3.1.3 Plasma Cleaner

The next sample preparation step is using a plasma cleaner. The CS-1701 plasma cleaner located in the CAMCOR semiconductor room creates a hydrophilic surface on the samples. Samples are placed inside the plasma cleaner with the windows facing upward. The samples undergo a 30% oxygen plasma clean for 30 seconds at 150 W.

3.1.4 Spin Coater

Next, to complete the first step in the e-beam lithography process of applying a resist, the headway research spin coater in CAMCOR is used. Spin coating is a process to apply a thin film on a surface. Basically, a flat object is held into place by a vacuum on a stage which spins rapidly to evenly distribute a liquid placed in the center of the object. In this case, the spin coater creates approximately an 18 nm layer of hafnium oxide sulfate (HafSOx) on the sample. HafSOx is a negative resist. The spin recipe consists of the following four steps with the ramp speed, final speed in revolutions per minute (rpm), and time:

1. 500 rpm/s, 3000 rpm, 10 s
2. 500 rpm/s, 0 rpm, 5 s

3. 500 rpm/s, 3000 rpm, 30 s

4. 500 rpm/s, 0 rpm, 0 s

After programming the spin recipe, the sample is placed on the chuck carefully to avoid placing windows directly above the vacuum hole. Next, the vacuum is turned on after making sure the vacuum line is open. Then, deionized (DI) water is placed on the entire sample to prevent windows from breaking during the first recipe step. During the second recipe step when the spin coater stops, HafSOx is applied with a filtered syringe to cover the entire sample. The syringe uses a 0.45 μm filter to prevent any slightly polymerized or chunky HafSOx from being deposited on the sample. The HafSOx is then spun in an even coat over the entire sample during the third recipe step. Edge effects are often observed and so larger samples (at least more than one 3.5 mm square sample) are preferable. After the spin recipe ends and the vacuum is turned off, the sample is immediately placed on a hot plate at 85 degrees Celsius for 1 minute. The soft bake is supposed to be at 80 degrees Celsius so the temperature is set at 85 degrees Celsius to reach the desired 80 degrees on the CAMCOR hotplates. After the soft bake, the sample is ready to be patterned. The sample is either patterned the same day or placed in a constant humidity box to preserve the HafSOx spin coat. Before patterning on the SEM, it is advisable to look at the sample again in the optical microscope to recheck that the windows to be patterned on are still intact.

3.1.5 Scanning Electron Microscope (SEM)

To complete the second step, exposure, of the e-beam lithography process a scanning electron microcope (SEM) is used. An SEM is a microscope which scans or rasters across an object with a focused beam of electrons. SEMs are generally used as imaging devices by detecting secondary electrons which are electrons emitted from atoms on the sample which have been excited by the focused electron beam. Yet, in this situation, the SEM is just used as a method to strategically expose a particular line pattern with the focused electron beam.

The CAMCOR Zeiss Ultra-55 SEM creates gratings with the Nanometer Pattern Generation System (NPGS) [16]. First, a pattern is made in Design CAD and saved as a *.dc2 file. A single pattern of a 30 μm by 30 μm area of 20 nm spaced lines is too large for the

computer to complete. To have a larger area pattern, two layers are made with lines spaced by 40 nm offset by 20 nm to result in a pattern over a 30 μm by 40 μm area with a 20 nm pitch.

The spin coated samples are placed in the SEM on a stage along with a standard gold nanoparticle sample. For patterning, a 30 kV beam and 7.5 μm aperture are used. First, the beam current which is normally around 25 pA must be recorded for the day. This value is entered in the NPGS run file editor before patterning. Then, the z-height is adjusted to get a working distance of about 4 mm and focus, wobble, and stigmation are corrected while examining the reference gold nanoparticles. The stage is moved near the windows to be patterned while being very careful not to expose more than just the corner or side of a window with the electron beam. Near each set of windows, the focus should be rechecked before patterning unless the NPGS xy-focus program is being used. Once well focused (able to resolve 5 nm features), the magnification should be at about 5000x with the screen centered on the corner of the window to be patterned. Then, the SEM screen should be frozen which means that the electron beam is no longer on so that the window is not accidentally exposed. NPGS mode is activated and then the run file editor can make the necessary adjustments such as changing the measured beam current and adjusting the center pattern location. The gratings are made with line doses of 0.8 nC/cm and 1 nC/cm. The line dose of 0.8 nC/cm is usually optimal and the 1 nC/cm line dose is tried to overdose the sample and create a smaller open fraction. Once the run file is ready, it is processed and the pattern is made on the sample with the electron beam. Since HafSOx is a negative resist, anywhere the electron beam exposes HafSOx is polymerized and therefore remains after development. After the pattern is made it is important to use direct stage control in the NPGS software to move the beam off the sample before switching back to SEM mode to find another window to pattern so that the entire window is not accidentally exposed. To assist in focusing and finding windows easily, scribe marks and colloidal carbon are helpful.

After patterning is complete in the SEM, the samples must be dipped for 30 seconds in 25% tetramethyl ammonium hydroxide (TMAH) for the development step in the lithography process. TMAH is a strong base and avoiding skin contact is very important. The TMAH etches away any HafSOx that was not exposed to electrons in the SEM. After the TMAH dip,

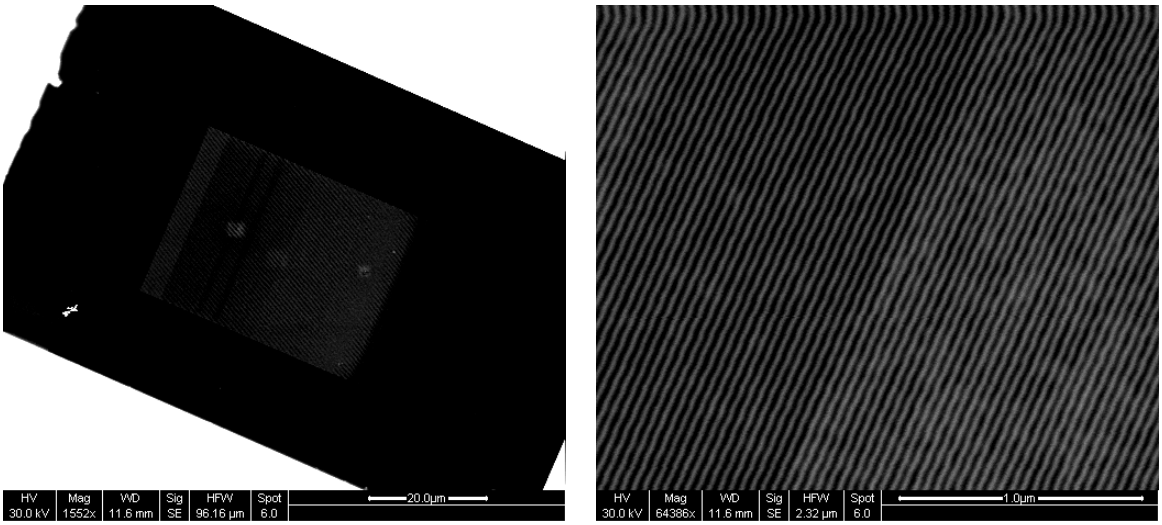

(a) An image of the window and pattern.

(b) An image of only the line pattern.

Figure 12: SEM images of a window after patterning. The HafSOx lines are visible in white with a 20 nm pitch.

the samples are rinsed well in DI water, blow dried with air and set on a 270 degrees Celsius hotplate for about three minutes for the hard bake. Once again, the optical microscope can be used to examine the samples for patterns as shown in Figure (11). Additionally, the gratings can be viewed with increased resolution using a SEM after fabrication as shown in Figure (12).

3.1.6 Carbon Coater

Silicon nitride is an insulator, which means that it becomes charged when exposed to electrons. Therefore, before examining the silicon nitride gratings in a TEM the samples must be coated in carbon to avoid becoming charged. The carbon coater in the CAMCOR semiconductor room applies approximately 20 nm of carbon to the back side of the samples.

3.1.7 Atomic Force Microscope (AFM)

The atomic force microscope provides height profile measurements. Figure (13a) displays an AFM image of a diffraction grating. The height profile measurements in Figure (13b) show that the gratings are only about 4.6 nm deep. Additional AFM measurements show

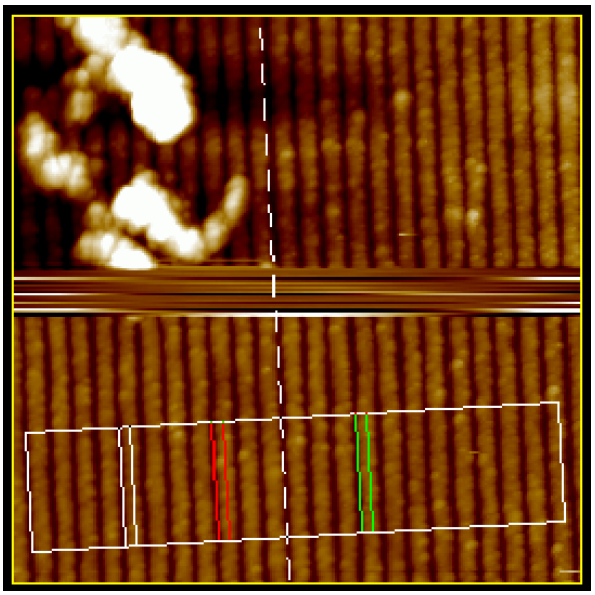

(a) An AFM image of a silicon nitride diffraction grating with contaminant in the top left corner and a computer malfunction in the center. Nevertheless, the image shows the desired line pattern.

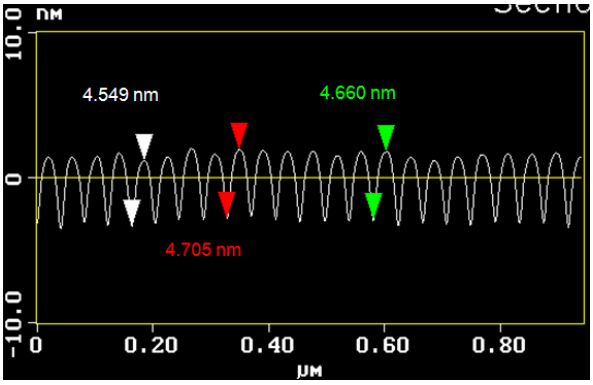

(b) The depth profile information from the AFM image in Figure (13a). The measurements suggest that the grating depth is only approximately 4.6 nm implying that the grating is of low efficiency since the spin coat is about 18 nm thick.

Figure 13: Images from an atomic force microscope of a 20 nm grating.

that the HafSOx spin coat layer is about 18 nm. Therefore, since the grating depth is only approximately 4.6 nm, it means that the samples were overexposed in the SEM because the desired pattern would have a grating depth of 18 nm. Additional dose tests would be necessary to increase the grating efficiency. Therefore, the AFM images and analysis suggest that other higher efficiency gratings would result in better Talbot effect observations because this grating would act as a phase grating not just an amplitude grating.

3.1.8 Transmission Electron Microscope (TEM)

The electron Talbot effect is experimentally investigated in the FEI Titan 80-300 transmission electron microscope (TEM) [14]. This TEM can accelerate electrons at 300 kV, which means that the electrons have an energy of 300 keV. In general, TEMs are useful because the short wavelength of the accelerated electrons allows for more spatial resolution than a light

microscope. A main way that a TEM differs from an SEM is that a TEM transmits electrons through a thin sample rather than detecting backscattered electrons from the sample. In our experiment, a diffraction grating is placed face down in the sample holder within the objective lens. Then, due to the interaction of the electrons transmitted through the grating an image can be seen on the fluorescent screen or captured by a CCD camera.

3.2 TEM Data Collection

The e-beam lithography sample fabrication process was completed many times with few successfully fabricated gratings. Many windows broke during the cleaning process because sonication causes 20 nm windows to shatter. This was an effect that was previously seen by SPI Supplies which sells silicon nitride membranes, but we unfortunately discovered the effect experimentally [17]. Additionally, the patterns in the SEM are sometimes not correctly placed on the windows. The reason for misplacing patterns is not fully understood, but this problem is resolved mainly by increasing the number of patterns attempted. Finally, 20 nm silicon nitride windows are fragile and so they do break as they age and are frequently handled. Unfortunately, even the windows which did appear to be patterned as desired showed a low efficiency in the AFM images. Due to the low efficiency of the e-beam lithography gratings, they are not used because they would not be ideal gratings to observe the Talbot effect.

Instead, higher efficiency gratings fabricated by Jordan Pierce, a graduate student in the McMorran lab group, are used. Jordan fabricates these gratings with the FEI Helios dual beam focused ion beam (FIB) using platinum deposition. In general, a FIB works similarly to an SEM except it uses an ion beam rather than an electron beam. In this particular case, the ion beam is not used to make the gratings. Instead the gratings are made by depositing rows of platinum within the FIB. This is a technique that Jordan has focused on to make high efficiency gratings. Figure (14) displays a representative image of the gratings used to obtain the electron Talbot effect images.

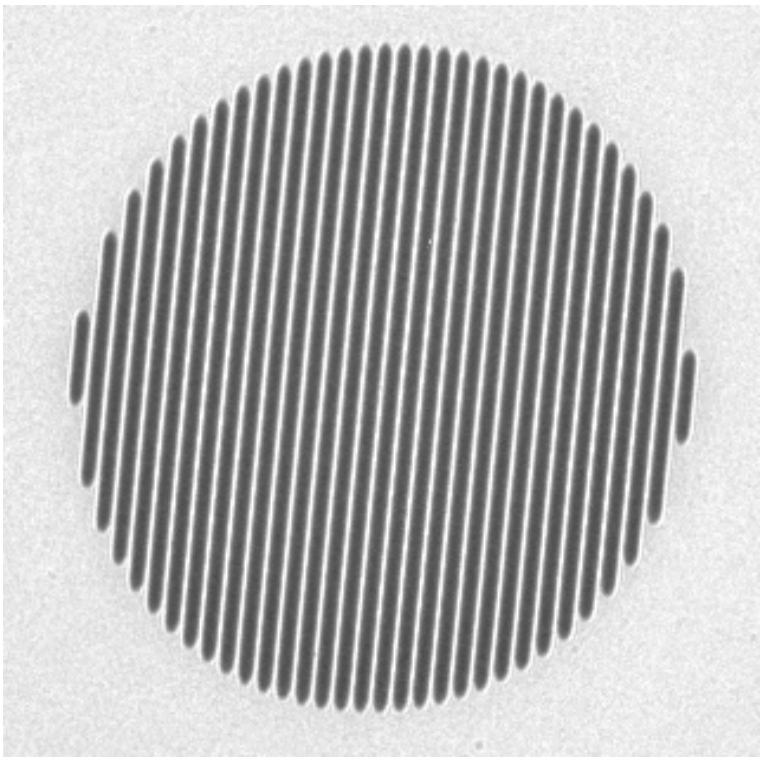

Figure 14: A TEM image of a 160 nm diffracting grating fabricated in the FIB using platinum deposition.

3.3 Electron Talbot Effect Results

To observe the electron Talbot effect, the TEM is used with one grating placed face down in the sample holder. The TEM control which adjusts the defocus of the image is used to view the Talbot revivals.

3.3.1 Images

First, the grating in the objective lens is focused on as shown in Figure (14). Then, a series of images are taken as the focus is changed. Image series range from -6 mm defocused to 6 mm defocused. In other words, images are taken from 6 mm below the grating to 6 mm above the grating. The diffraction gratings are all made with a FIB with stated pitches of 120 nm, 140 nm, and 160 nm. An example of an image series from in focus to defocusing through one Talbot length is shown in Figure (15). The stated fractional Talbot lengths

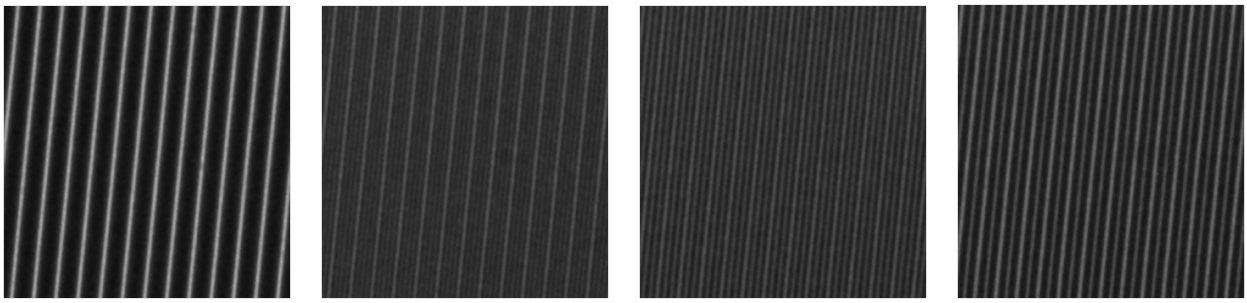

(a) In focus at 0.0 L_T (b) 4x lines at 0.27 L_T (c) 3x lines at 0.39 L_T (d) 2x lines at 0.52 L_T

(e) 3x lines at 0.71 L_T (f) 4x lines at 0.75 L_T (g) 1x lines at 1 L_T

Figure 15: A TEM image series obtained by starting in focus and defocusing to one Talbot length using a 160 nm pitch grating to show the fractional Talbot revivals.

in Figure (15) are calculated by defining the first visible Talbot revival as 1 L_T and then number of images between in focus and the image of interest is divided by the total number of images between in focus and 1 L_T. The theoretical Talbot length for the 160 nm pitch grating in Figure (15) is 12.99 mm. Yet, according to the TEM defocus reading, the first Talbot revival appeared at 5.19 mm. To explain this discrepancy, line profiles of the 160 nm grating are obtained using Fiji. The method to estimate the real grating pitch in Fiji is shown in Figure (16). This method basically entails drawing a line, creating a line profile and visually estimating the pitch. Table (1) displays estimated grating pitches calculated by averaging at least five line profiles. Additionally, the table shows the theoretical Talbot lengths based on the stated grating pitch and estimated grating pitch to compare with the experimental Talbot length. The experimental Talbot lengths are calculated by dividing the total defocus distance of the TEM by the total number of images taken multiplied by the number of images in one Talbot length.

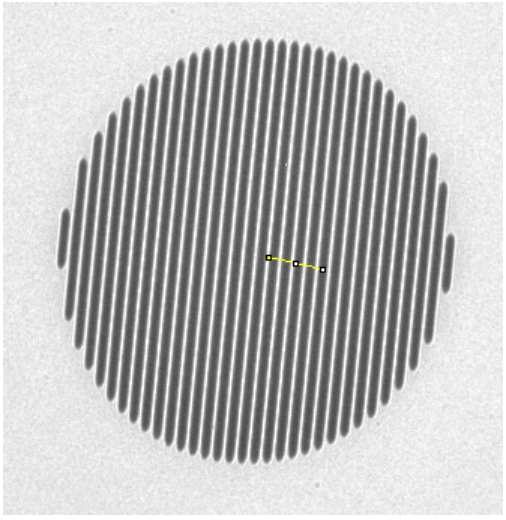

(a) 160 nm grating image in Fiji with the yellow line drawn to calculate the line profile in Figure (16b).

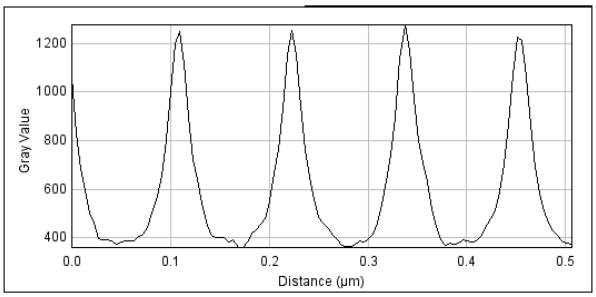

(b) Line profile for the grating shown in Figure (16a) showing a periodicity of about 111 nm.

Figure 16: A 160 nm grating and it's line profile calculated in Fiji to show that it's grating pitch can be estimated to be near 111 nm.

Stated grating pitch (mm)	Estimated grating pitch (mm)	Theoretical L_T with stated pitch (mm)	Theoretical L_T with estimated pitch (mm)	Experimental L_T (mm)
160	111	12.99	6.25	5.19
140	100	9.95	5.08	3.87
120	84	7.31	3.58	3.23

Table 1: Table of stated and visually estimated grating pitches along with theoretical and experimental Talbot lengths for comparison.

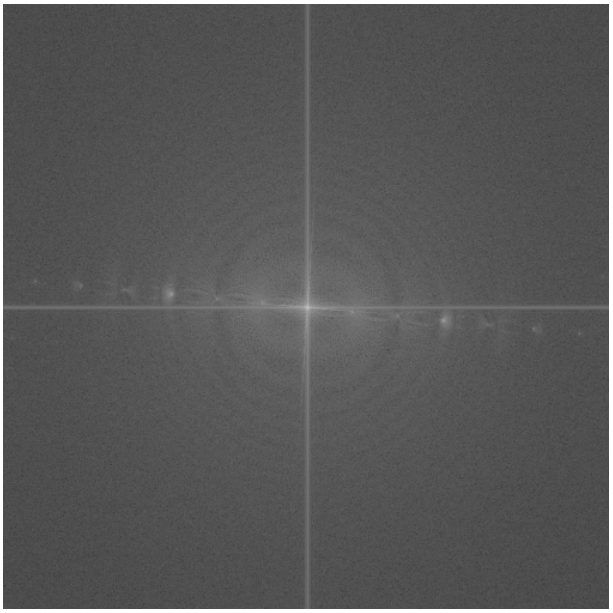

Figure 17: An example FFT of a period three Talbot revival which shows the third dots from the center as the brightest.

The difference in the stated grating pitch and estimated grating pitch leads to very different predicted Talbot lengths. Yet, the estimated grating pitch leads to closer theoretical and experimental Talbot lengths than the stated grating pitch. For instance, for the 160 nm pitch grating the percent error between the theoretical Talbot length and experimental Talbot length is only 17.1% for the estimated pitch whereas the percent error is 60.1% for the stated pitch. Therefore, it is reasonable to assume that the stated grating pitches are inaccurate. Thus, there remain only minor discrepancies between the theoretical and experimental Talbot lengths. Some of the error is likely from visual estimation of both the grating pitch and identifying exactly which Talbot images represent Talbot revivals to calculate the experimental Talbot length. These human errors likely do not explain all of the discrepancy, but more experiments would need to be conducted. If the discrepancies remain, gratings with very accurately known pitches could be used to calibrate built-in TEM defocus functions.

3.3.2 Fast Fourier Transforms (FFTs)

To better explain and quantify the changes in periodicity which occur due to the Talbot effect as seen in Figure (15), fast Fourier transforms (FFTs) are done on the images. FFTs are a way to do Fourier transform on a two dimensional data set. This is a procedure to identify if frequency is present. The FFTs are done in Fiji on different visible periodicities and then line profiles are taken of the FFTs to analyze them. Figure (17) displays what a FFT of a period three image looks like. The important feature to note is that the third dots away from the center are the brightest since it is a FFT of a period three Talbot revival.

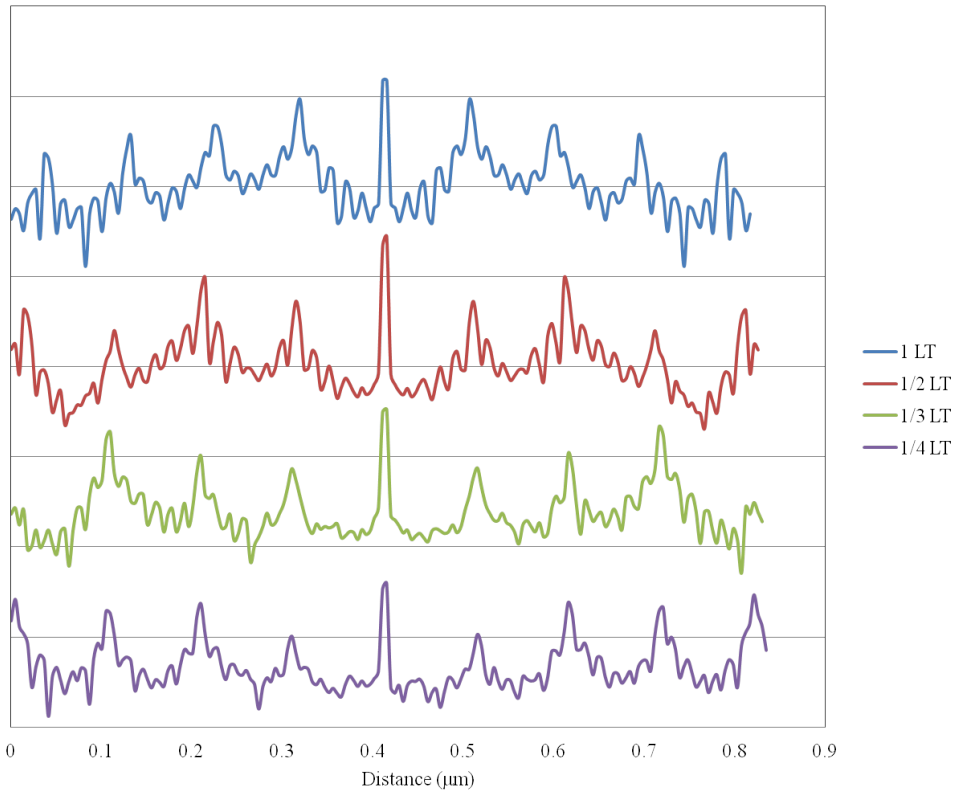

Figure 18: Line profiles of FFTs at one Talbot length, a quarter Talbot length, a third Talbot length, and half a Talbot length showing that they all have equal periodicities but the maximum peak position corresponds to the fractional Talbot length revival.

To compare the FFTs of different periodicties, line profiles are taken of many FFTs. All the FFTs had approximately the same period (dot spacing) of about 100 nm. Yet, the

difference between FFTs of different periodicities is which dots are the brightest or showed up as the highest peaks in the line profiles. To see this phenomenon, Figure (18) shows line profiles of different FFTs. For example, at a third of the Talbot length, the third peaks are the tallest which corresponds to the bright third dots seen in Figure (17). This analysis confirms the qualitative doubling, tripling, and quadrupling which is visible at fractional Talbot lengths.

4 Conclusion

The experimental results of both the optical and electron Talbot effect are in good agreement with the theorized results. In the future, further experiments investigating the Talbot Lau effect can be completed. Better images could be obtained at one Talbot length and period doubling images could be obtained as well. Additionally, further work with the electron Talbot effect in the TEM should be completed with a more accurately known grating pitch. Then, the experimental results could actually be used to calibrate the TEM defocus function. Finally, the Talbot effect and nanoscale gratings could be used to create smaller features. To do this, a precisely made stand could hold perhaps a 20 nm pitch grating at half a Talbot length above a sample to be patterned in an SEM. Then, the electron beam could be scanned over the entire grating and since the grating below is at half a Talbot length, the exposure would lead to twice the periodicity of the top grating resulting in a pitch of only 10 nm. Similarly, if the top grating was placed at a quarter Talbot length, then the new grating pitch would be only 5 nm. These would be fairly simple experiments to execute with the resources of CAMCOR at University of Oregon. Other light sources, such as X-rays, could be investigated as well especially for medical applications. For example, X-ray Talbot interferometry (XTI) is of interest as a phase imaging possibility [9].

References

[1] *The world of physics* (2012), URL http://sites.psu.edu/passionmalencia/2012/12/08/things-get-weird/.

[2] *Fresnel diffraction* (2014), URL http://en.wikipedia.org/wiki/Fresnel_diffraction.

[3] H. Talbot, Philosophical Magazine Series 3 **9**, 401 (1836), http://dx.doi.org/10.1080/14786443608649032, URL http://dx.doi.org/10.1080/14786443608649032.

[4] R. Wild, *The Talbot effect* (2005), URL http://www.atomwave.org/otherarticles/wildthesis2.pdf.

[5] M. S. Chapman, C. R. Ekstrom, T. D. Hammond, J. Schmiedmayer, B. E. Tannian, S. Wehinger, and D. E. Pritchard, Phys. Rev. A **51**, R14 (1995), URL http://link.aps.org/doi/10.1103/PhysRevA.51.R14.

[6] B. J. McMorran and A. D. Cronin, New Journal of Physics **11**, 033021 (2009), URL http://stacks.iop.org/1367-2630/11/i=3/a=033021.

[7] M. R. Dennis, N. I. Zheludev, and F. J. G. de Abajo, Opt. Express **15**, 9692 (2007), URL http://www.opticsexpress.org/abstract.cfm?URI=oe-15-15-9692.

[8] A. A. Maradudin and T. A. Leskova, New Journal of Physics **11**, 033004 (2009), URL http://stacks.iop.org/1367-2630/11/i=3/a=033004.

[9] A. Momose, W. Yashiro, Y. Takeda, Y. Suzuki, and T. Hattori, Japanese Journal of Applied Physics **45**, 5254 (2006), URL http://stacks.iop.org/1347-4065/45/i=6R/a=5254.

[10] K. Patorski (Elsevier, 1989), vol. 27 of *Progress in Optics*, pp. 1 – 108, URL http://www.sciencedirect.com/science/article/pii/S0079663808700842.

[11] J. Wen, Y. Zhang, and M. Xiao, Adv. Opt. Photon. **5**, 83 (2013), URL http://aop.osa.org/abstract.cfm?URI=aop-5-1-83.

[12] W. B. Case, M. Tomandl, S. Deachapunya, and M. Arndt, Opt. Express **17**, 20966 (2009), URL http://www.opticsexpress.org/abstract.cfm?URI=oe-17-23-20966.

[13] *Transmission electron microscopy* (2014), URL http://en.wikipedia.org/wiki/Transmission_electron_microscopy.

[14] *FEI* (2014), URL http://www.fei.com/products/tem/titan/.

[15] *CAMCOR Oregon's High-Tech Extension Service* (2014), URL http://camcor.uoregon.edu/.

[16] *Zeiss* (2014), URL http://www.zeiss.com/microscopy/en_us/products/scanning-electron-microscopes/ultra-materials.html.

[17] *Spi supplies brand silicon nitride window grids for tem* (2013), URL http://www.2spi.com/catalog/grids/silicon-nitride.php.